(4)

CHEMISTRY - STRUCTURE - PROPERTY INTERRELATIONSHIPS FOR CALCAREOUS DEPOSITS AS STAND ALONE COATINGS (Second Year)

ONR Contract N00014-86-K-0144

FLORIDA ATLANTIC UNIVERSITY
College of Engineering • Department of Ocean Engineering
Center for Marine Materials

(4)

Annual Report

CHEMISTRY - STRUCTURE - PROPERTY INTERRELATIONSHIPS FOR CALCAREOUS DEPOSITS AS STAND ALONE COATINGS (Second Year)

ONR Contract N00014-86-K-0144

submitted to

Office of Naval Research
800 North Quincy Street
Arlington, Virginia 22217

submitted by

W. H. Hartt, S. W. Smith, J. S. Luo
R. U. Lee and T. Y. Chen

Center for Marine Materials
Florida Atlantic University
Boca Raton, Florida 33431

September 30, 1988

ABSTRACT

Calcareous deposits which formed in natural sea water upon ASTM A710 steel polarized either potentiostatically, galvanostatically or by a mixed mode technique (initially galvanostatic followed by potentiostatic) have been studied. Parameters investigated included variation of current density (potentiostatic control) or potential (galvanostatic control) with time, total charge transfer, deposit thickness, thickness-to-charge ratio, deposit morphology and deposit composition.. Based upon these the mixed mode technique was judged to provide the deposit with greatest protective properties within the time frame of the experiments. This appears to be related to nature of the initial, magnesium-rich film established during the preliminary, experimental period; and the mechanism of calcareous deposit formation is discussed within this context.

INTRODUCTION

A unique feature of cathodic protection in sea water is formation of calcareous deposits on metal surfaces. Advantageous aspects of these deposits, such as decrease in cathodic current requirement have been investigated by various authors, (1-5); and from this the formation mechanism has been projected in general terms to involve (a) an increase in pH of electrolyte adjacent to the metal surface due to either or both of the reactions

$$1/2\ O_2 + H_2O + 2e \text{ -----> } 2OH^- \quad \text{and} \qquad [1]$$

$$2\ H_2O + 2e \text{ -----> } H_2 + 2OH^-, \quad [2]$$

b) enhanced carbonate ion concentration according to

$$HCO_3^- + OH^- \text{ -----> } H_2O + CO_3^- \quad \text{and} \quad [3]$$

c) precipitation of inorganic compounds whose solubility product is exceeded, such as

$$Ca^{+2} + CO_3^{-2} \text{ -----> } CaCO_3 \text{ and} \quad [4]$$

$$Mg^{+2} + 2OH^- \text{ -----> } Mg(OH)_2. \quad [5]$$

Historical investigations have considered various property versus parameter relationships, including composition-current density (1,6), morphology-potential (7), applied current density-protective current density (8), composition-temperature (4), current requirement-temperature (9) and current density-potential (5).

In the present study specific attention has been focused upon the relative effect of type of polarization (potentiostatic, galvanostatic or a mixed galvanostatic-potentiostatic mode) upon properties of the resultant calcareous deposits. Thus, for the potentiostatic polarization mode current density and, hence, hydroxide ion formation rate should decrease with time due to calcareous deposit development and resultant oxygen concentration polarization. For galvanostatic polarization, however, the hydroxide ion production rate remains constant with time. Because reactions [1]-[5] above are interrelated, it was anticipated that polarization mode distinction could influence the composition, structure and properties of calcareous deposits, as characterized by parameters such as current density (potentiostatic) or potential (galvanostatic) decay, total charge transfer, thickness and morphology.

EXPERIMENTAL PROCEDURE

The electrochemical cell, which is illustrated in Figure 1, was based upon a series of conventional 600 ml beakers utilizing non-recirculated, sand filtered, natural sea water as is available at the Center Laboratory as the electrolyte. Properties for this sea water, including salinity, conductivity and concentration of critical species such as calcium, magnesium, organics and pH have been historically monitored; and some of these have been reported for an annual cycle (10). The electrode was a 12.7mm diameter cylinder machined from 25.4mm plate with the axis in the rolling plane. Specimen preparation involved polishing with 600 grit SiC paper and ultransonic cleaning sequentially in acetone and distilled water. Steel composition is listed in Table I, and a more complete detailing of microstructure and mechanical properties has been presented elsewhere (11). For cathodic polarization the specimen was mounted in a PTFE holder as shown in Figure 2.

Polarization was based upon a circular, platinum coated niobium counter mesh electrode, a saturate calomel reference electrode (SCE) and locally fabricated potentiostats/galvanostats. Potentiostatic control involved potentials of -800, -900 and -1000 mV (SCE), whereas galvanostatic experiments were performed at 250, 300 and 350 mA/m^2. The mixed mode procedure involved initial galvanostatic polarization until potential decreased to -900 mV, at which time control was shifted to potentiostatic at this same potential. Deposit thickness was determined by before-and-after measurement of specimen diameter using a micrometer that provided six micrometer resolution. Duration

of all experiments was 7000 minutes.

Morphological analyses were performed using an ISI Super IIIA Scanning Electron Microscope, and deposit composition was evaluated using an EG&G Ortec System 5000 energy dispersive x-ray analyzer. For consistency all geometric parameters of the specimen and detector were maintained constant during the compositional analysis phase.

RESULTS AND DISCUSSION

Current Density and Potential versus Exposure Time. Figures 3 and 4 present the results for the potentiostatic and galvanostatic experiments, respectively. In the former case, current density decay was in general accord with trends reported previously (5,9), while for the latter the rate of potential decrease was relatively constant and the same for each of the three current densities, subsequent to the initial, relatively sharp decline. After 7000 minutes the potential for all galvanostatic experiments was more negative than -1000 mV. The top half of Figure 5 represents the initial galvanostatic phase whereas the bottom represents the subsequent potentiostatic phase.

Results for the combined mode experiments are presented in Figure 5. In subsequent discussions a notation of the form 250/900 has been employed to identify these; where the first three digits indicate the magnitude of current density in the initial galvanostatic phase and the last three the absolute value for potential (mV) during the subsequent, potentiostatic portion. As should be intuitively expected the time to reach -900 mV decreased with increasing current density during galvanostatic polarization. For example, at 250mA/m^2 a

potential of -900 mV was reached after approximately 2000 minutes, whereas, only about four minutes were required with 350 mA/m^2. Upon switching from galvanostatic to potentiostatic control, a drop in current density between 10 mA/m^2 (250/900 experiment) and 30 mA/m^2 (350/900 experiment) occurred. However, after a few minutes the current densities of the galvanostatic phases were resumed.

Visual Observations. Specimens polarized potentiostatically to -800 mV exhibited localized, greenish discoloration after 4000 minutes of exposure. Similar observation was made for the 250 mA/m^2 galvanostatic specimens. Upon exposure to the atmosphere these areas turned brown, suggesting that the polarization had not completely precluded anodic dissolution.

Based upon appearance, deposits were divided into two distinct groups; one of grayish white color and the other milky white. All the specimens that achieved -1000 mV or more negative (-1000 mV potentiostatic and all galvanostatic specimens) were in the latter category (milky white color), whereas -900 mV potentiostatic and all mixed mode specimens belong to the former. Apparently, this distinction reflected a sufficiently high polarization level in the former case so that deposits spalled in response to hydrogen evolution.

SEM Observations. Figures 6-8 present micrographs of deposits formed potentiostatically at -800, -900 and -1000 mV, respectively. Thus, in the former case (-800 mV) coverage does not appear complete. On the other hand, a dense scale of fine columnar particles was formed

at -900 mV. For -1000 mV (Figure 8) the deposit was also dense, although coalescence was incomplete and overall particle size was greater than at -900 mV. Figures 9-11 show micrographs for deposits formed on galvanostatically polarized specimens (250, 300 and 350 mA/m^2, respectively) and illustrate that particle size variations were relatively modest and well with an order-of-magnitude of one another. Also, an increasing tendency for cracking and spalling of the coating with increased polarization is apparent from Figures 9-11, as should be expected in the potential regime of hydrogen gas evolution (Figure 4). For the mixed mode cases Figures 12-14 indicate that particles were relatively fine and, as for the galvanostatic case, was independent of the polarization parameters. Despite the fact that the deposit formation process apparently involved nucleation and growth of individual particles, the appearance of the spalled material suggested that the growth impingement process provided adequate lateral strength that the film behaved as a single structural unit.

In instances where observations could be made between individual deposit particles, a sublayer was apparent as illustrated by Figure 15. These fine fiber-like constituent particles were best resolved at magnifications above 600 X. Presence of this sublayer was not confirmed for the -900 mV potentiostatic and 350/900 mixed mode experiments. This was attributed to the completeness of surface coverage by the outer deposit.

Compositional Analysis. The results of EDX analyses are presented in Table II and revealed that with the exception of the -800 mV potentiostatic experiment calcium was the predominant deposit

component detected. This contrasts with early results of Humble (1), who found that Ca-Mg ratio decreased with increasing current density. On the other hand, analysis of sublayers (see above) revealed these to be relatively concentrated with magnesium, as shown in Table III. Detection of iron was believed due to penetration of the electron beam to the steel substrate and not necessarily to the presence of this species in deposits.

Total Charge. Results for computation of total charge transferred during the course of the three types of experiments are reported in Table IV. This reveals that, while total charge increased with increasing magnitude of polarization in both the potentiostatic and galvanostatic experiments, the mixed mode procedure resulted in an inverse dependence of this parameter upon current density during the galvanostatic phase.

Deposit Thickness. The results of deposit thickness measurements are presented in Table V. As should be expected, thickness increased with increasing cathodic polarization, irrespective of polarization mode (potentiostatic or galvanostatic). This same trend extended to the mixed mode case also, such that film thickness increased in proportion to the magnitude of current density during the initial galvanostatic period. This indicates that that film thickness does not necessarily vary in proportion to total charge, since the highest mixed mode current density yielded the least total charge and greatest film thickness for this control procedure.

Thickness-to-Charge Ratio. The above trends have been investigated in terms of the ratio of deposit thickness to total charge. An inherent assumption to attaching significance to this parameter is that the thickness measurement reflects the quantity of deposit formed and not a change in density. A listing of ratios is given in Table VI, which indicates that values near unity typify deposits formed during purely potentiostatic and galvanostatic experiments. For the mixed mode case, however, the ratio increased in proportion to the magnitude of the initial, galvanostatic current density with the greatest value (1.9 μm/Coul.) corresponding to 350/900. Apparently, the relatively brief, constant current period (approximately four minutes) during this experiment had an important, beneficial effect upon ultimate properties of the deposit, as exemplified by both the highest thickness to charge ratio and the lowest final current density (see Figure 5).

Morphological Considerations: The observations pertaining to particle size (Figures 6-14) must be related to classical nucleation rate theory coupled with the influence of magnesium ions in sea water upon calcium carbonate precipitation. Thus, a process of solid phase precipitation, from an aqueous solution, followed by growth, can yield either an increasing or decreasing particle size with increasing level of supersaturation depending upon the relative role of heterogeneous versus homogeneous nucleation and the efficiency of the catalyzing heterogeneous nucleation process (12). The present situation is modified, however, by the complex influence of sea water composition. Thus, while near-surface sea water is supersaturated with $CaCO_3$ (13),

it is undersaturated with $Mg(OH)_2$; and precipitation of the latter is possible only for pH greater than approximately 9.3 based upon K_{sp} (apparent) = 2.4×10^{-11} (14). Supersaturation of $Mg(OH)_2$ can arise, however, in response to cathodic polarization as a consequence of the production of OH^- at cathodic sites (Equations [1] and [2]). Because pH decreases continuously from the metal surface it is expected that supersaturation of $Mg(OH)_2$ occurs only within a certain distance from the metal surface. Beyond this point sea water is supersaturated with $CaCO_3$ only. The observation that the sublayers formed adjacent to the steel surface were magnesium rich and the outer layers were calcium rich, can be explained by this pH gradient.

With regard to $CaCO_3$ it is generally recognized that calcite is the most stable form for this species in sea water (15). However, precipitation from solution is either inhibited or retarded by Mg^{+2} and organic compounds in seawater (16). Consequently, although aragonite is thermodynamically less stable than calcite, its relative occurrence is facilitated by kinetics factors (17). While, Mg^{+2} does retard nucleation of aragonite, it does not inhibit growth (15). In relatively high cathodic current density situations it has been projected that precipitation of $Mg(OH)_2$ results in depletion of Mg^{+2} within the diffusional boundary layer (18), thereby facilitating $CaCO_3$ precipitation. Consistent with the projection of Kunjapur et al (4), the plateau in either current density (Figures 3 and 5) or potential (Figures 4 and 5) may reflect an incubation period for the formation of $CaCO_3$ subsequent to the initial $Mg(OH)_2$ film achieving a steady state thickness. In summary, the observed dominance of Mg in the sublayers is associated with the high pH condition near the metal

surface and the inhibition or retardation of $CaCO_3$ formation by Mg^{+2} present in sea water.

The above rationale suggests that the nucleation rate of calcareous deposits should increase in proportion to the magnitude of cathodic polarization. However, there is no consistent trend apparent from Figures 6-14 indicating that this was the case. One possible explanation is that in the present case, where deposits grew for 7,000 minutes, evolutionary factors concealed nucleation site densities. Also, for the mixed mode procedure deposits may have been primarily influenced by the second component, potentiostatic phase, which was identical in all cases. Thus, a common morphology is not unexpected here. On the other hand, comparison of deposit morphologies from the -900 and -1000 mV pure potentiostatic experiments reveals a clear contrast with the nucleation rate-magnitude of polarization trend projected above. A possible explanation for this is that nucleation rate and ultimate particle size were influenced by properties of the initially formed magnesium rich film.

Significance of Magnesium Rich Deposits: The observation that charge efficiency was greatest for deposits formed at the highest initial current density of the mixed mode test condition (350/900) has important implications. Note for example from Figure 5 that slope of the current density-time curves from the potentiostatic phase of these experiments is approximately the same in each case and also equal to that for the -900 mV purely potentiostatic case (Figure 3). This suggests that protective character of deposits formed during the

post-galvanostatic period of the mixed mode experiment was the same, irrespective of current density during the galvanostatic phase. Thus, the distinction between the various mixed mode experiments is that data for the potentiostatic portion of the 350/900 experiment was displaced from the outset by approximately -100 mA/m^2 compared to the purely potentiostatic case; and this factor was responsible for enhancing charge efficiency. Also, the film formed during the initial galvanostatic period of the 350/900 experiment apparently resulted in an approximate two-fold increase in charge-to-thickness ratio, although the time frame for this to occur was only four minutes. A subsequent experiment was performed where a calcareous deposit was developed galvanostatically at 350 mA/m^2 and terminated after four minutes. Analysis of this film indicated magnesium to be the only cation present. (Table III)

Historical research addressing cathodic protection in sea water and calcareous deposits has suggested that magnesium rich deposits provide poor protection compared to calcium rich ones (1,19). Thus, Culberson (19) potentiostatically polarized mild steel specimens to -900 mV in simplified, synthetic sea waters using a cell and rotating cylinder generally similar to that of the present experiments (rotation speed 58 rpm). For a solution containing only sodium and magnesium salts (no calcium) current density subsequent to film formation was 30 times greater than for a solution of sodium and calcium salts alone (no magnesium). Using the same procedure as Culberson (19), Kunjapur et al (4) found that the deposits present after 300 minutes of polarization to -900 mV in natural sea water were magnesium rich and provided no apparent current density reduction

compared to the initial value. These latter experiments, however, did not focus upon the short-time, current density trends.

From the present experiments two aspects of the galvanostatically formed, magnesium rich film are important. Thus, charge-to-thickness ratio should be maximized by an initial film which 1) polarizes the metal to -900 mV in the briefest period and 2) results in the lowest current density upon polarization to -900 mV. Figure 5 indicates that lower current densities existed at conclusion of the 300 and 250 mA/m^2, compared to 350 mA/m^2, galvanostatic phases of the mixed mode experiments; however, charge-to-thickness ratio was dominated by the relative times required to achieve -900 mV. This suggests that as high an initial current density as feasible should be employed in the galvanostatic phase of the mixed mode procedure; however, little additional benefit may be realized by further reducing the four minutes required to polarize to -900 mV with a current density of 350 mA/m^2. Figure 16 presents a plot of the initial current density-time data for the purely potentiostatic -900 mV experiment and shows that current density exceeded 350 mA/m^2 for the initial 15 minutes of exposure. Thus, either the constant current condition promoted development of a more protective deposit during the initial period or optimum properties resulted from an intermediate current density.

CONCLUSIONS

1. Calcareous deposits consist of two layers: The outer layer is comprised of columnar or globular particles and the inner layer (sublayer) comprised of fine fibrous particles. EDX results show that the latter is magnesium rich whereas the former is dominated by calcium.

2. Formation of Mg rich sublayer is the result of initial, high pH adjacent to the metal surface and the inhibition or retardation of $CaCO_3$ formation by Mg^{+2} present in sea water. Outside the sublayer pH is lower than necessary for $Mg(OH)_2$ saturation. Consequently, Ca dominates in the outer layer.

3. The mixed mode, especially 350/900 polarization (initially galvanostatic followed by potentiostatic) provided a deposit with the greatest protective properties, judged from current density, deposit thickness and thickness-to-charge ratio. This is attributed to the rapid formation of an initial, magnesium rich sublayer.

BIBLIOGRAPHY

1. R. A. Humble, Corr., 4, p. 358, 1948.

2. I. A. Denison and M. Romanoff, Corr., 9, p. 132, 1953.

3. H. S. Preiser and B. T. Silverstein, J. Am. Soc. Naval Eng., 62, p. 881, 1950.

4. M. M. Kunjapur, W. H. Hartt and S. W. Smith, Corrosion 43, p. 674, 1987.

5. S. L. Wolfson and W. H. Hartt, Corrosion, 37, p. 70, 1981.

6. H. Klas, Arch. Eisenhuetten, 29, p. 321, 1958.

7. V. D. Pirogov, Yu.L. Kuz'min and A. P. Zhuk, Zashchita Metallov, 9, p. 311, 1973, English translation in Protection of Metals.

8. V. P. Grigorev and S.Ya Popov, Zhurnal Prikladnoi Khimi, 35, p. 1621, 1962, English translation in Journal of Applied Chemistry of the USSR.

9. G. C. Clapp, The Effect of Temperature on the Formation of Calcareous Deposits on Mild Steel Under Cathodic Protection, M.S. Thesis, University of Manchester, 1978.

10. W. H. Hartt, "Fatigue of Welded Structural Steel in Sea Water", Paper No. 3962, 1981 Offshore Technology Conference, May 4-7, Houston, 1981.

11. W. H. Hartt and S. S. Rajpathak, "Fatigue of Selected High Strength Steels in Sea Water - A Compilation of Materials Properties," Center for Marine Materials Report to API, Sep. 1, 1987.

12. A. G. Walton, The Formation and Properties of Precipitates, Wiley Interscience, New York, 1967.

13. K. E. Chave and E. Suess, Limnol. Oceanogr., 15, p. 633, 1970.

14. R. M. Pytkowicz and R. Gates, Science 161, p. 690, 1968.

15. R. A. Berner, Geochim. Cosmochim. Acta, 39, p. 489, 1975.

16. R. M. Pytkowicz, J. Geol., 73, p. 196, 1965.

16. K. E. Chave, Sci., 143, p. 1723, 1965.

17. J. L. Bischoff, J. Geophys. Res. 73, p. 3315, 1972.

18. S. H. Lin and S. C. Dexter, "Effects of Temperature and Magnesium Ions on Cathodic Protection," Proceedings of the Sixth (1987) International OMAE Symposium, Vol. III, p.431.

19. C. H. Culberson, "Effect of Sea Water Chemistry on the Formation of Calcareous Deposits", Paper No. 61, Corrosion '83.

TABLE I

Chemical composition of the ASTM A710 specimen

Element	Wt. %	Element	Wt. %	Element	Wt. %
C	0.04	Ni	0.82	B	0.0001
Si	0.30	Cr	0.67	Ti	0.002
Mn	0.45	Mo	0.18	Al	0.034
P	0.004	Nb	0.037	Fe	96.3122
S	0.002	V	0.004		
Cu	1.14	N	0.0047		

Table II

EDX analysis of calcareous deposits

	Potentiostatic (mV)			Galvanostatic (mA/m^2)			Mixed Mode		
	-800	-900	-1000	250	300	350	250/ 900	300/ 900	350/ 900
Fe	74.3	5.9	7.1	24.0	1.6	1.3	9.0	7.2	3.4
Na	9.2	8.3	5.3	3.9	7.5	5.1	4.9	8.6	6.4
Ca	3.4	82.0	83.7	66.2	84.3	90.0	80.7	78.7	85.4
Mg	8.6	0.6	1.4	3.2	1.3	1.4	1.6	1.4	-
Cl	2.1	1.9	0.9	2.7	2.5	0.9	2.1	2.0	3.9
Si	2.0	0.6	1.0	-	1.5	1.0	0.9	1.5	0.8
Sr	0.3	0.8	0.7	-	1.2	0.9	0.8	0.6	0.3

Table III

EDX analysis of calcareous deposit sublayers

	Potentiostatic (mV)			Galvanostatic (mA/m^2)			Mixed Mode		
	-800	-900	-1000	250	300	350	250/ 900	300/ 900	350/ 900
Fe	76.32	-	76.02	72.30	6.76	0.52	55.08	76.72	-
Na	8.89	-	9.36	8.75	4.78	4.70	15.41	4.82	-
Ca	0.29	-	4.32	1.85	3.89	4.16	3.43	3.96	-
Mg	11.15	-	6.48	14.62	66.94	73.85	17.56	11.57	-
Cl	0.39	-	0.63	2.24	8.45	8.05	3.48	1.08	-
Si	2.05	-	2.55	0.23	3.97	3.22	2.16	1.61	-
Sr	0.35	-	0.65	-	0.86	0.50	0.52	0.24	-
K	-	-	-	-	-	-	2.37	-	-

TABLE IV

Total charge

Polarization	Condition	Total Charge (Coul.)
Potentio-static	- 800 mV	33.8
	- 900	89.6
	-1000	137.8
Galvano-static	250 mA/m^2	105
	300	126
	350	147
Mixed	250/900	86.7
	300/900	76.7
	350/900	62.6

TABLE V

Mean deposit thickness

Polarization Mode	Condition	Deposit Thickness (μm)
Potentio-static	- 800 mV	40
	- 900	90
	-1000	170
Galvano-static	250 mA/m^2	100
	300	140
	350	170
Mixed	250/900	80
	300/900	110
	350/900	120

TABLE VI

Thickness-to-charge ratio

Polarization Mode	Condition	Thickness-to-Charge (μm/Coul.)
Potentio-static	- 800 mV	1.2
	- 900	1.0
	-1000	1.2
Galvano-static	250 mA/m^2	1.0
	300	1.1
	350	1.1
Mixed	250/900	1.0
	300/900	1.5
	350/900	1.9

FIGURE CAPTIONS

1. The electrochemical cell.

2. Specimen assembly.

3. Current density vs. time behavior for potentiostatic polarization.

4. Potential vs. time behavior for galvanostatic polarization.

5. Mixed mode polarization. The top half represents the initial galvanostatic polarization and the bottom half the following potentiostatic polarization at -900 mV.

6. SEM micrograph of deposit potentiostatically formed -800 mV. (Original magnification x120)

7. SEM micrograph of deposit potentiostatically formed -900 mV. (Original magnification x120)

8. SEM micrograph of deposit potentiostatically formed -1000 mV. (Original magnification x120)

9. SEM micrograph of deposit galvanostatically formed at 250 mA/m^2. (Original magnification x120)

10. SEM micrograph of deposit galvanostatically formed at 300 mA/m^2. (Original magnification x120)

11. SEM micrograph of deposit galvanostatically formed at 350 mA/m^2. (Original magnification x120)

12. SEM micrograph of deposit formed by mixed mode polarization, initial 250 mA/m^2 followed by -900 mV. (Original magnification x120)

13. SEM micrograph of deposit formed by mixed mode polarization, initial 300 mA/m^2 followed by -900 mV. (Original magnification x120)

14. SEM micrograph of deposit formed by mixed mode polarization, initial 350 mA/m^2 followed by -900 mV. (Original magnification x120

15. Same as Figure 11, except higher magnification x600.

16. Initial current density vs. time behavior for potentiostatic polarization at -900 mV.

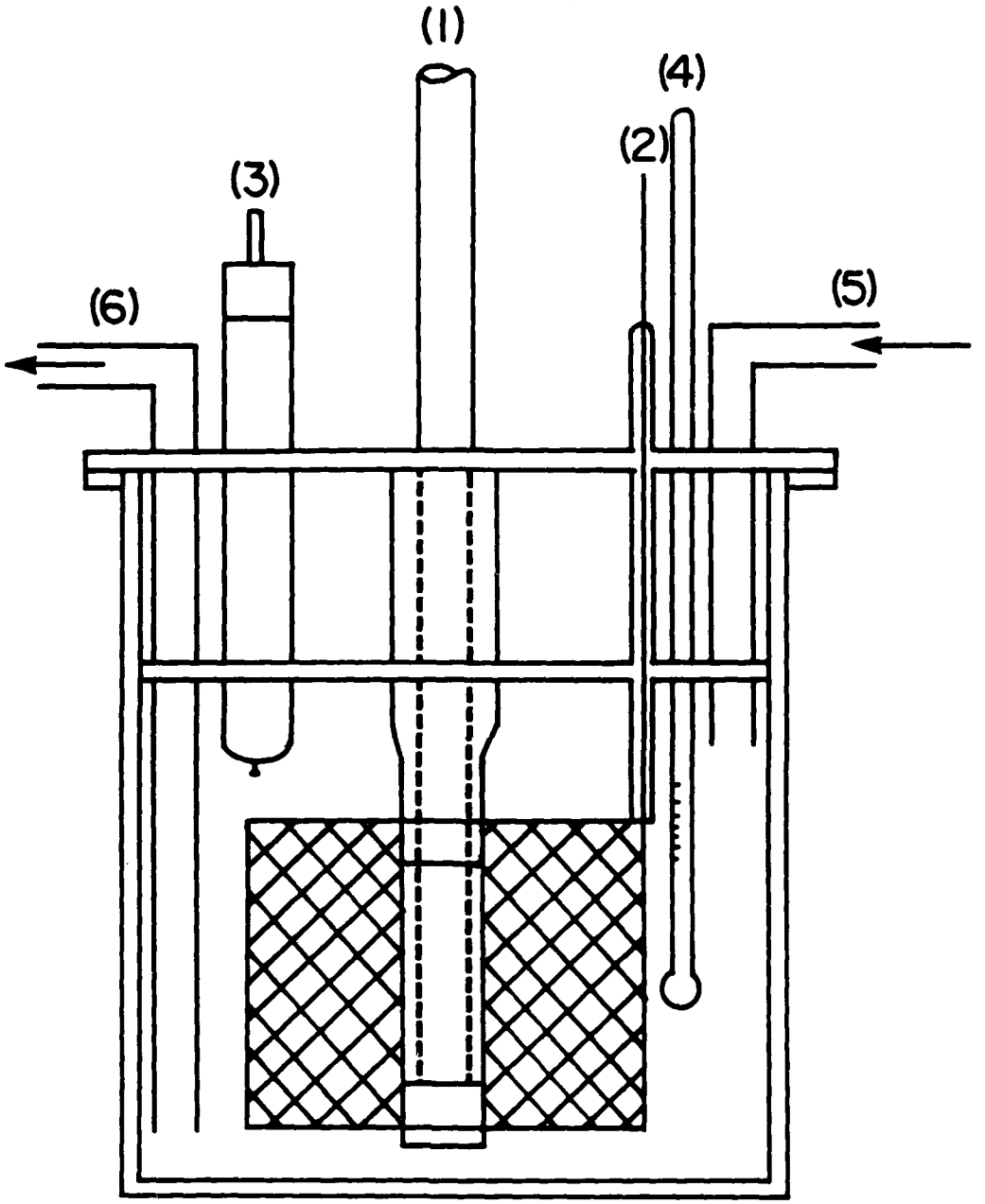

1). Specimen Holder
2). Counter Electrode
3). Reference Electrode
4). Thermometer
5). Solution Inlet
6). Solution Outlet

FIGURE 1. ELECTROCHEMICAL CELL.

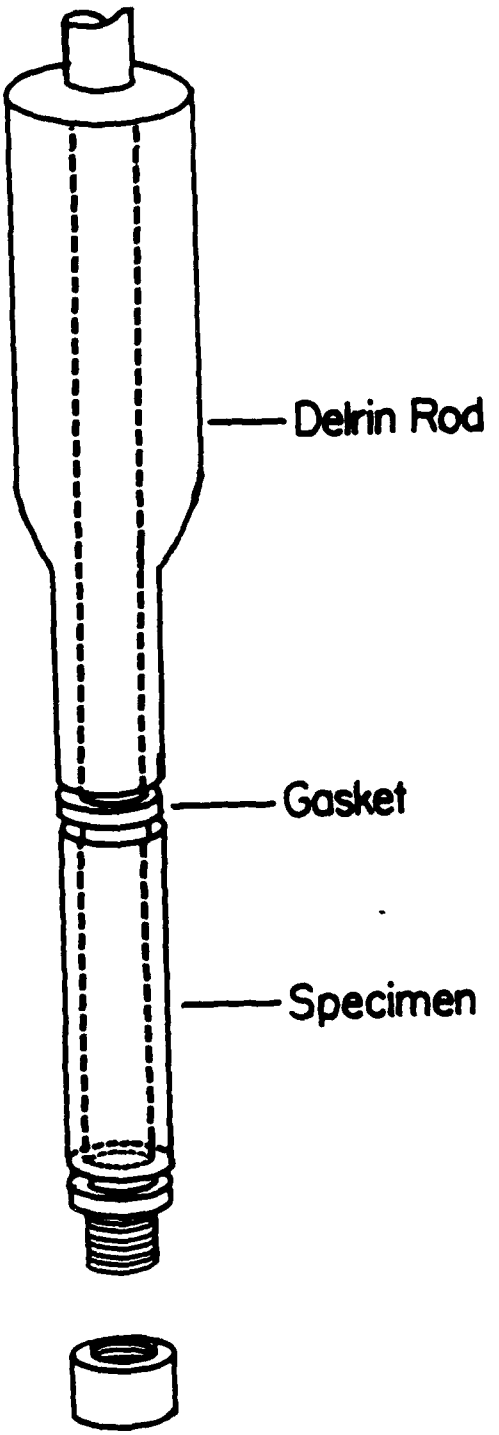

FIGURE 2. SPECIMEN HOLDER.

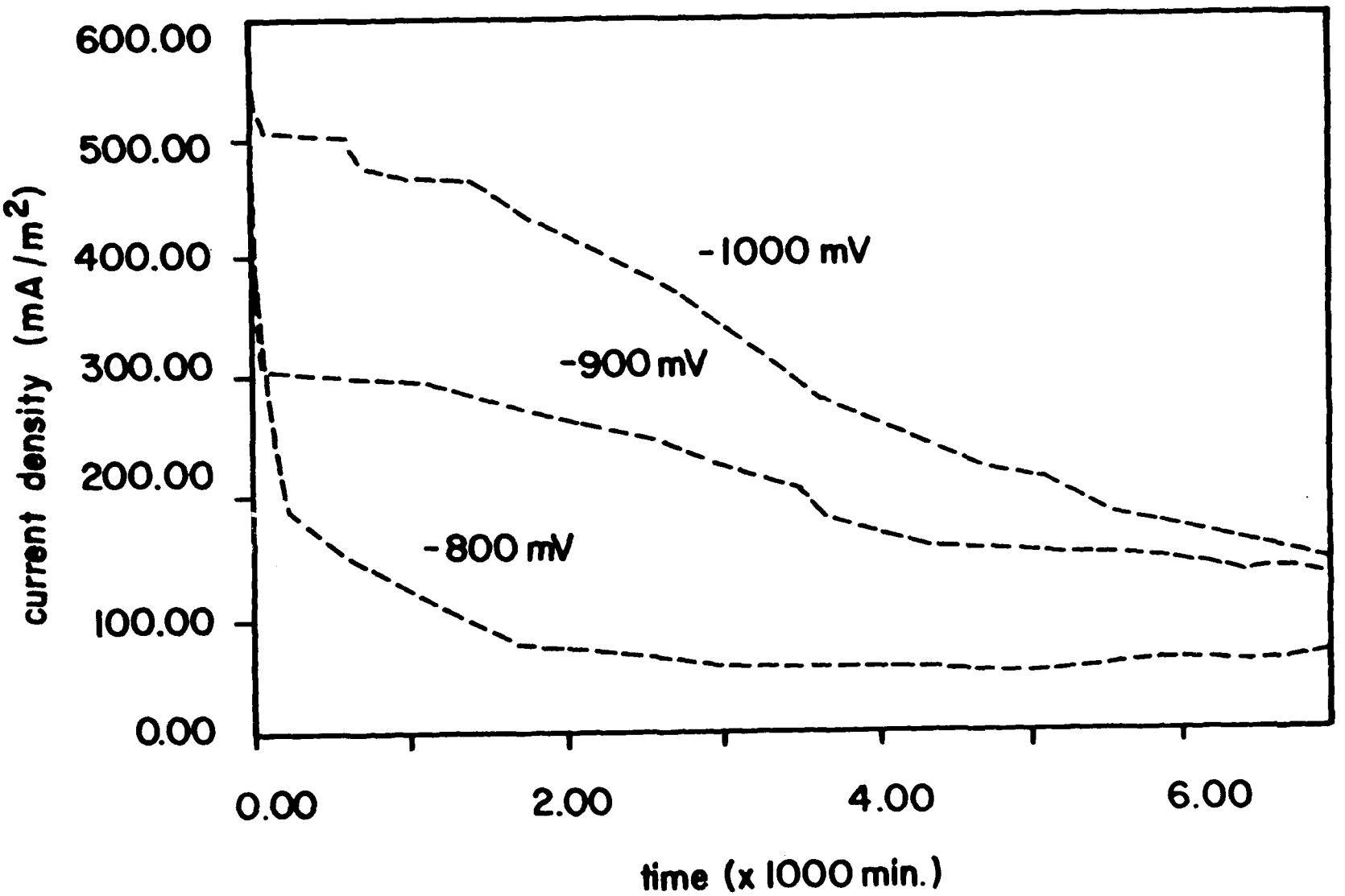
600.00
500.00
400.00
300.00
200.00
100.00
0.00
current density (mA/m²)
-1000 mV
-900 mV
-800 mV
0.00
2.00
4.00
6.00
time (x 1000 min.)

Figure 3

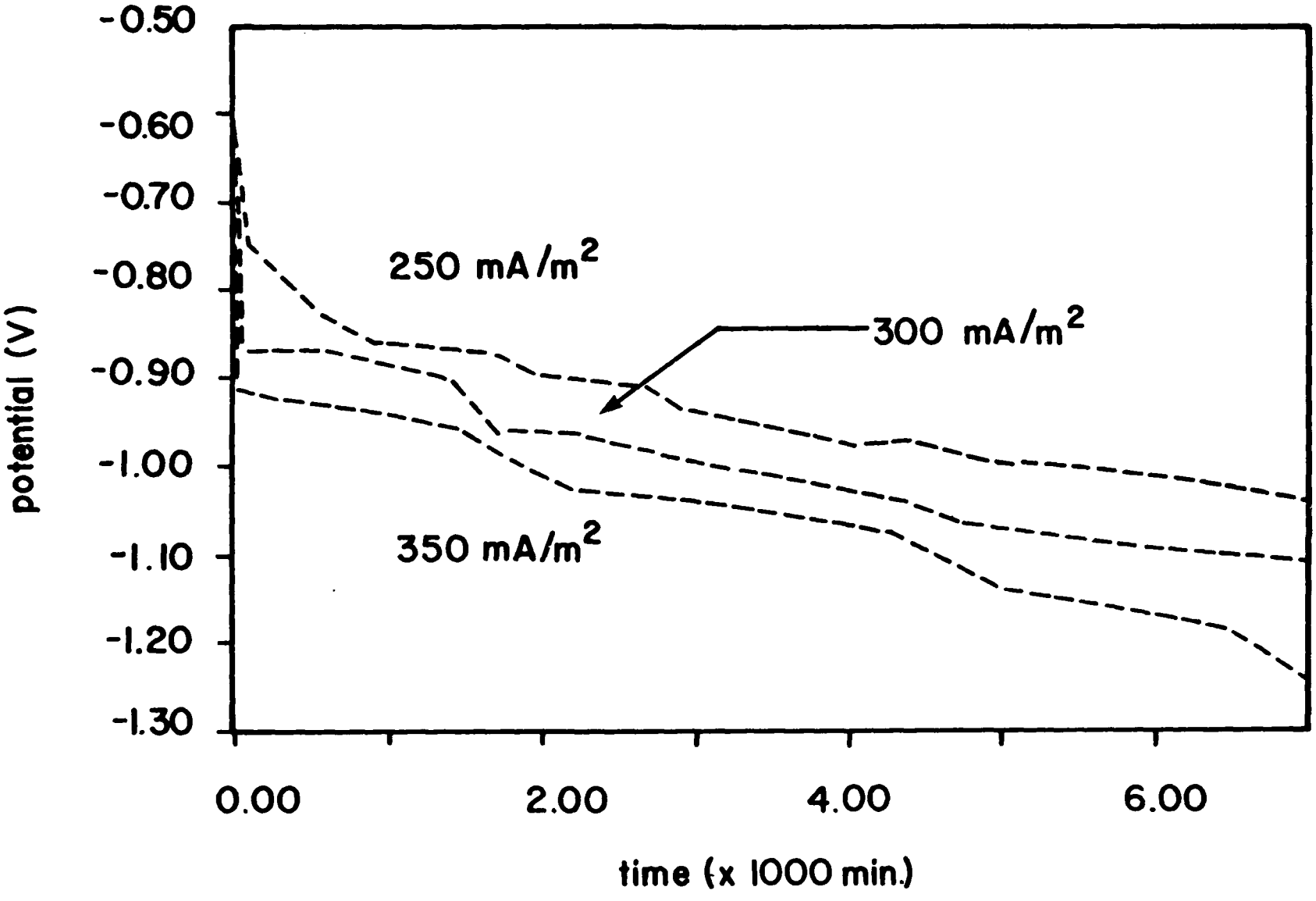
-0.50
-0.60
-0.70
-0.80
-0.90
-1.00
-1.10
-1.20
-1.30
potential (V)
250 mA/m2
300 mA/m2
350 mA/m2
0.00
2.00
4.00
6.00
time (x 1000 min.)

Figure 4

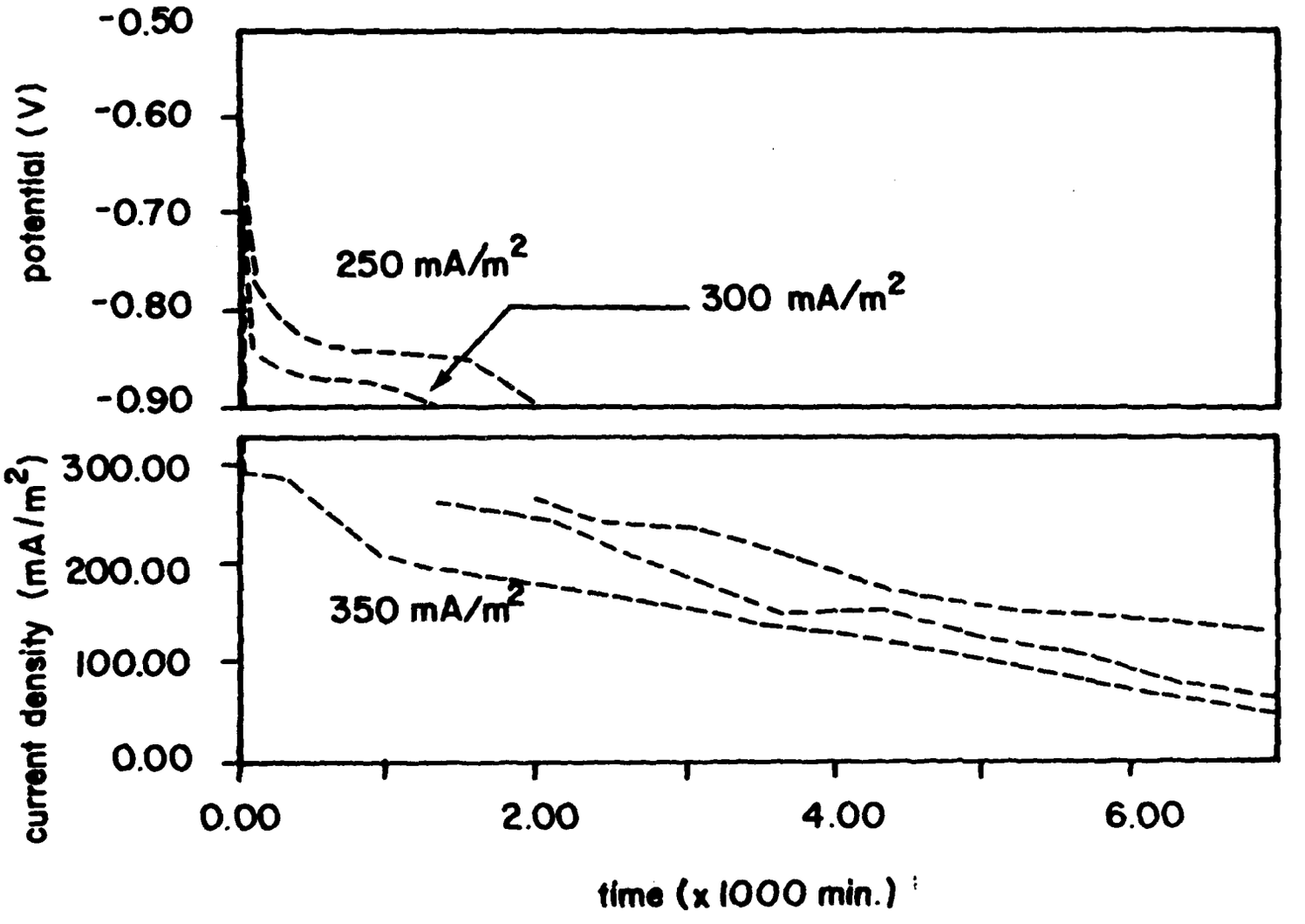
-0.50
-0.60
-0.70
-0.80
-0.90
potential (V)
250 mA/m2
300 mA/m2
300.00
200.00
100.00
0.00
current density (mA/m2)
350 mA/m2
0.00
2.00
4.00
6.00
time (x 1000 min.)

Figure 5

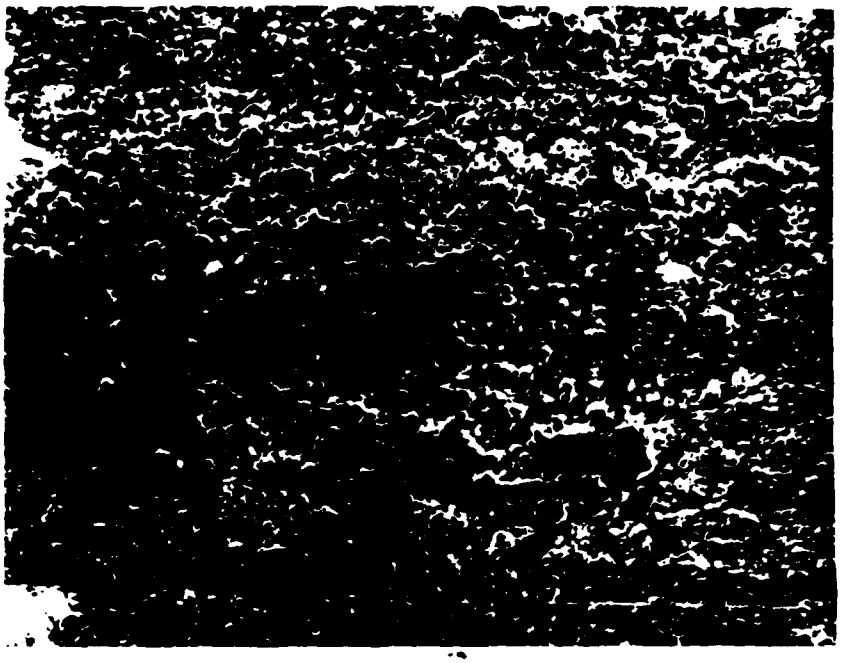

Figure 6

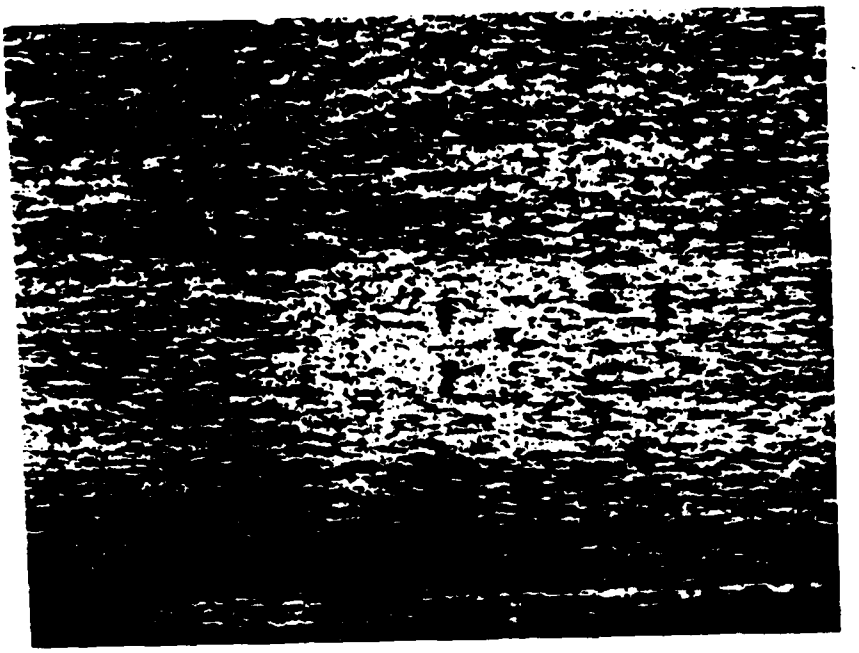

Figure 7

Figure 8

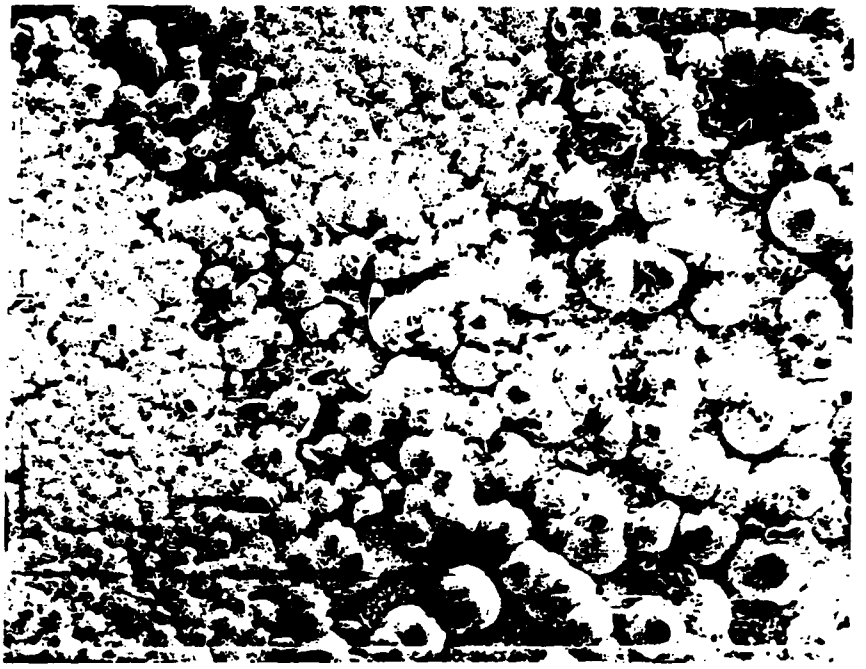

Figure 9

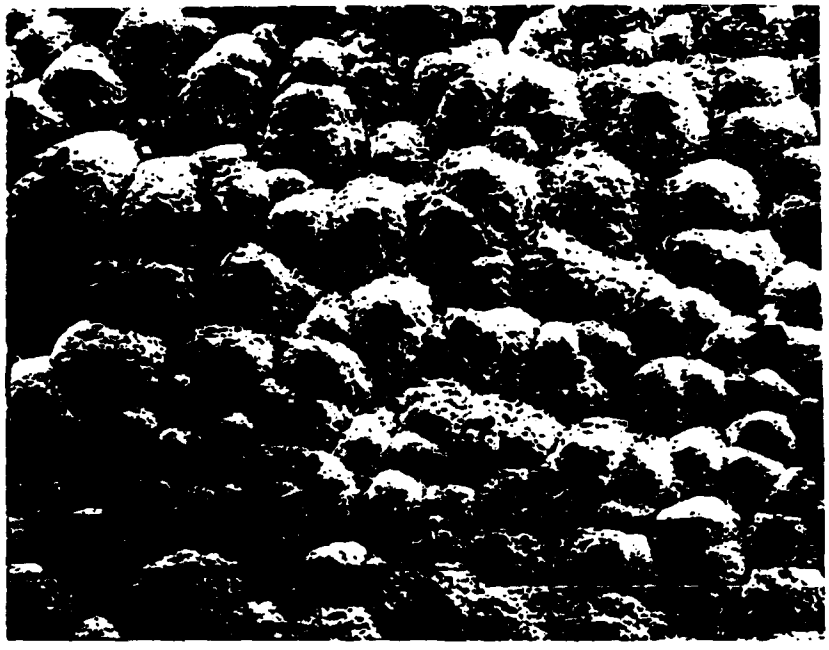

Figure 10

Figure 11

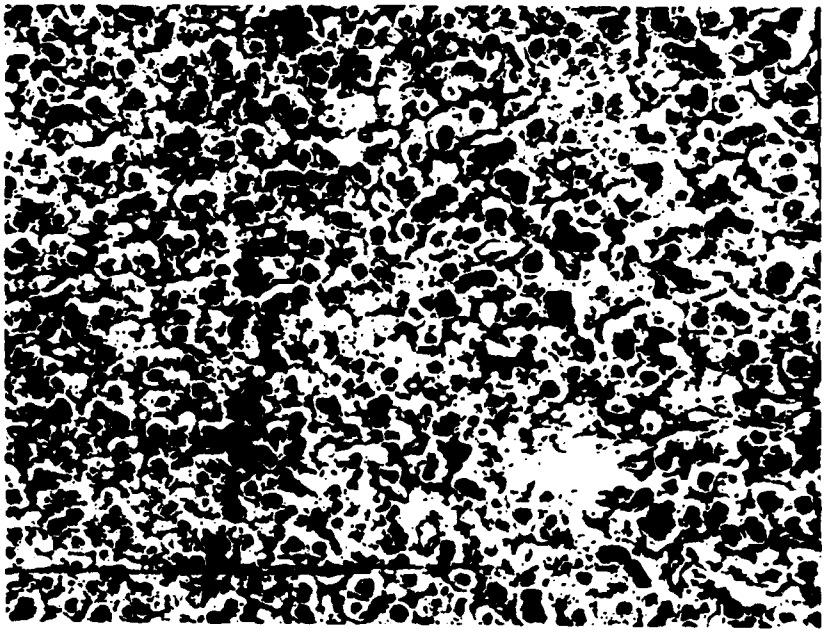

Figure 12

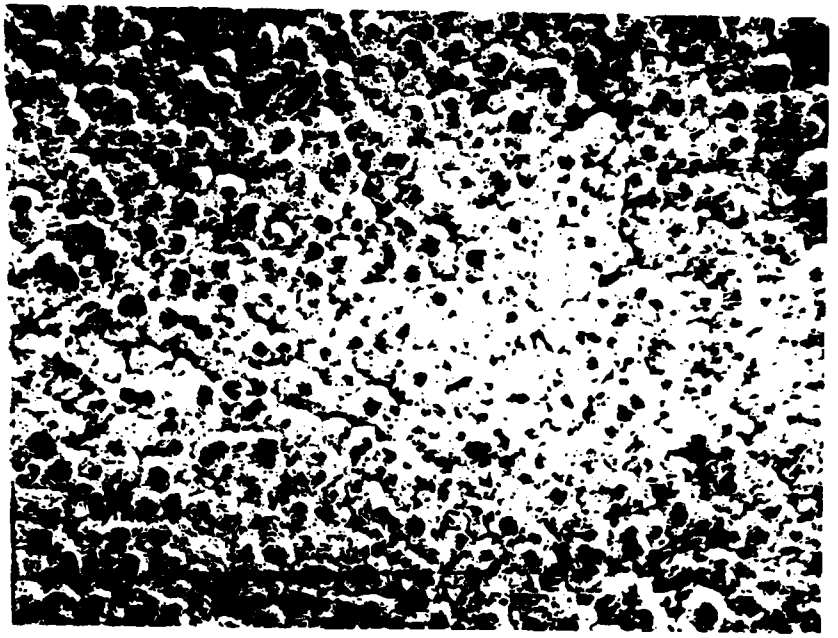

Figure 13

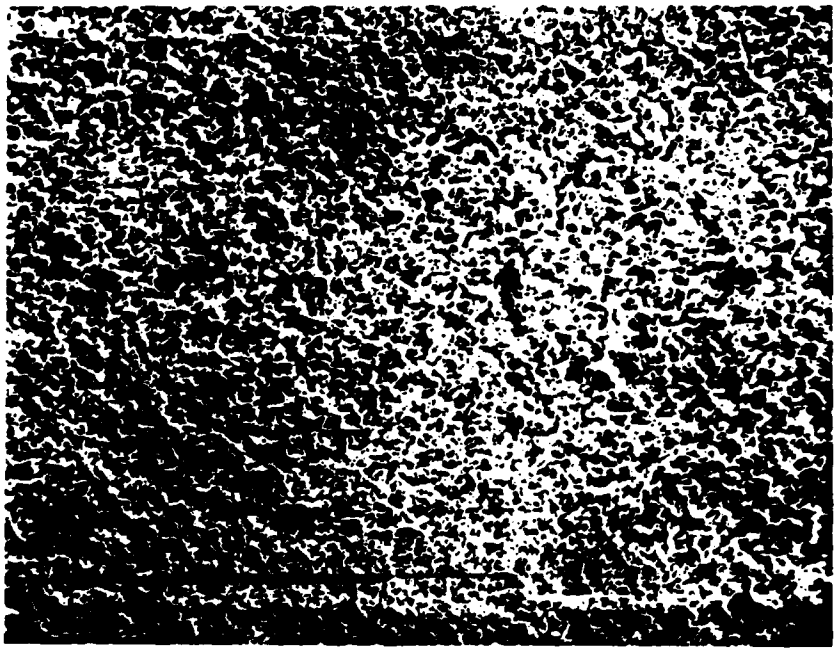

Figure 14

Figure 15

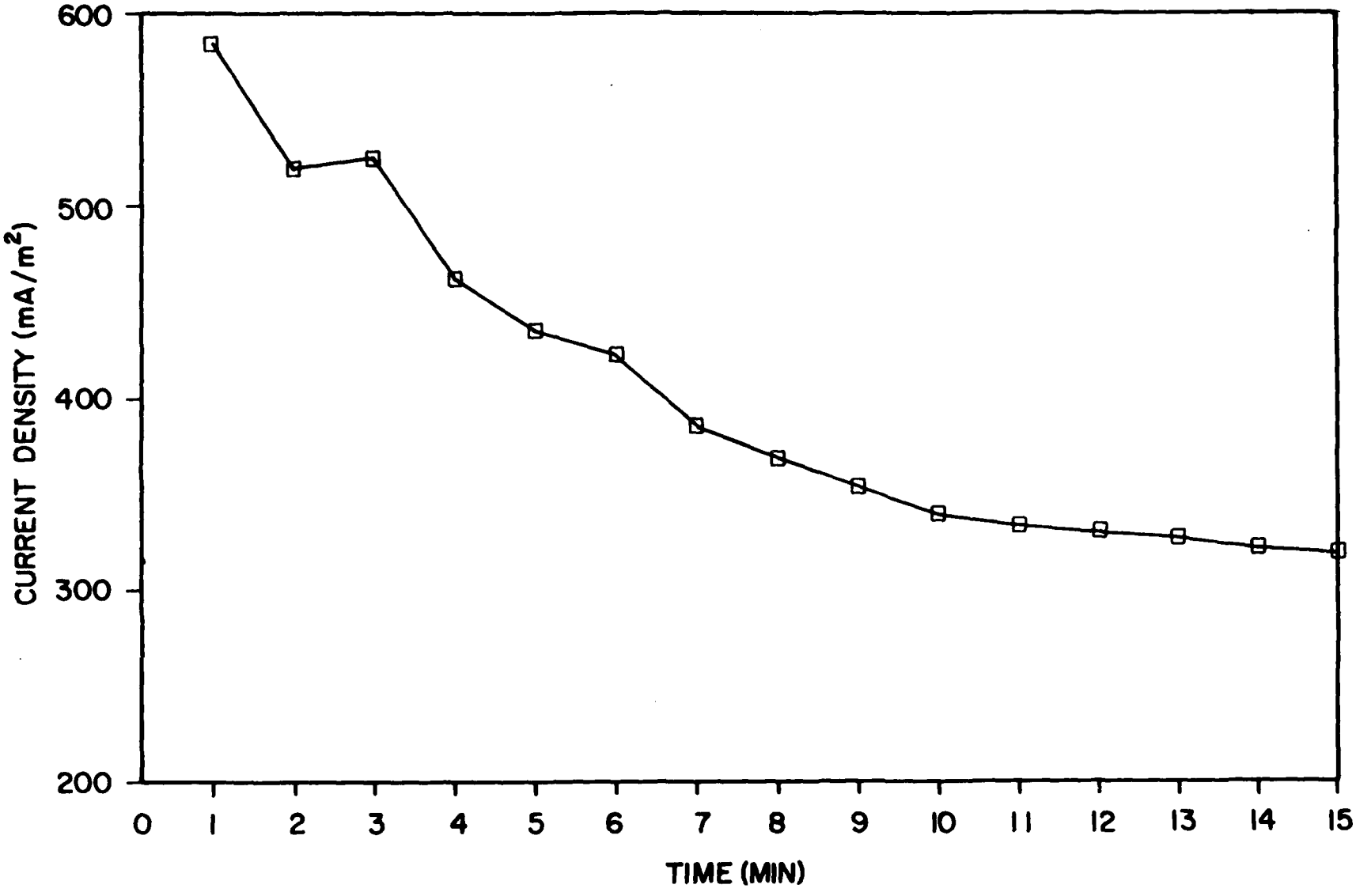
600
500
400
300
200
CURRENT DENSITY (mA/m²)
0
1
2
3
4
5
6
7
8
9
10
11
12
13
14
15
TIME (MIN)

Figure 16